

Supporting Information

Stereo effects for efficient synthesis of orange-red multiple resonance emitters centered on a pyridine ring

Mingxu Du,^a Minqiang Mai,^a Dongdong Zhang,^a Lian Duan,^a and Yuewei Zhang,^{*bc}

^aKey Lab of Organic Optoelectronics and Molecular Engineering of Ministry of Education, Department of Chemistry, Tsinghua University, Beijing 100084, P. R. China.

^bLaboratory of Flexible Electronics Technology, Tsinghua University, Beijing 100084, P. R. China.

E-mail: zhangyuewei@mail.tsinghua.edu.cn

^cApplied Mechanics Lab, School of Aerospace Engineering, Tsinghua University, Beijing 100084, P. R. China.

1. Experimental Section

1.1 General Information. All commercially available reagents were used as received unless otherwise stated. All reactions were carried out using Schlenk techniques under a nitrogen atmosphere. 400 MHz ^1H -NMR and 150 MHz ^{13}C -NMR spectra were measured by a JEOL JNM-ECS600 spectrometer at room temperature in deuterated dichloromethane and chloroform respectively with tetramethyl silane as the internal standard. MALDI-TOF-MS data was performed on a Shimadzu AXIMA Performance MALDI-TOF instrument in positive detection modes. Elemental analyses were performed on a flash EA 1112 spectrometer.

1.2 Single-Crystal Structure. Diffraction data were collected on a Rigaku R-AXIS-RAPID diffractometer using the ω -scan mode with graphite-monochromator $\text{Mo}\cdot\text{K}\alpha$ radiation. The structure determination was solved with direct methods using the SHELXTL programs and refined with full-matrix least squares on F2. The corresponding CCDC reference number (2297213) and the data can be obtained free of charge from The Cambridge Crystallographic Data Centre via www.ccdc.cam.ac.uk/data_request/cif.

1.3 Computational methods. The calculations were performed using the Gaussian 16 package,^{S1} employing density functional theory (DFT) and time-dependent density functional theory (TD-DFT) methods. The B3LYP and PBE0-D3BJ hybrid functionals were utilized.^{S2-5} The structures were optimized based on the single-crystal structure or optimized structure. Franck-Condon analyses of the absorption/emission spectra were performed according to the previous literature.^{S6}

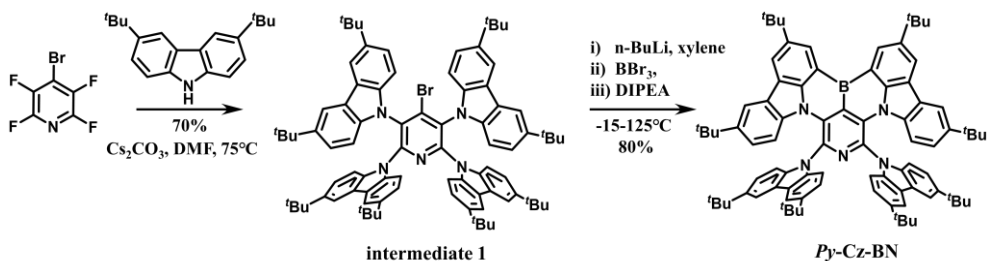
1.4 Photoluminescence Property Measurements. The concentration of the solution (1×10^{-5} M) was prepared by stepwise dilution for solution state measurements. Thin films for photophysical characterization were prepared by thermal evaporation on quartz substrates at $1\text{-}2 \text{ \AA sec}^{-1}$ in a vacuum chamber with a base pressure of $< 10^{-5}$ torr. UV-vis absorption and PL spectra were measured using UV-2600 (Shimadzu) and FluoroMax-4P (Horiba) instruments at 77 and 298 K. The PLQYs were obtained with an absolute photoluminescence quantum yield measurement system Hamamatsu

C9920-03G in an integrating sphere. The solution sample was bubbled with nitrogen for 10 minutes before measurement while the films were measured in air. The transient spectra were collected on an Edinburgh Fluorescence Spectroscopy FLS1000.

1.5 Electrochemical measurements. The electrochemical properties of *Py-Cz-BN* were studied by cyclic voltammetry. As shown in Fig. S10, the oxidation potentials calculated from the onset of the oxidation curves are -4.01 eV and -1.87 eV for *Py-Cz-BN*, vs. an Fc/Fc^+ standard, corresponding to the highest occupied molecular orbital (HOMO) and lowest unoccupied molecular orbital (LUMO) levels of -4.82 eV and -2.68 eV for *Py-Cz-BN*, using ferrocene as a reference.

1.6 Device fabrication and measurement of EL characteristics. All compounds were subjected to temperature-gradient sublimation under high vacuum before use. OLEDs were fabricated on the ITO-coated glass substrates with multiple organic layers sandwiched between the transparent bottom indium-tin-oxide (ITO) anode and the top metal cathode. Before device fabrication, the ITO glass substrates were pre-cleaned carefully. All material layers were deposited by vacuum evaporation in a vacuum chamber with a base pressure of 10^{-6} torr. The deposition system permits the fabrication of the complete device structure in a single vacuum pump-down without breaking vacuum. The deposition rate of organic layers was kept at 0.1 - 0.2 nm s^{-1} . The doping was conducted by co-evaporation from separate evaporation sources with different evaporation rates. The current density, voltage, luminance, external quantum efficiency, electroluminescent spectra and other characteristics were measured with a Keithley 2400 source meter and an absolute EQE measurement system in an integrating sphere at the same time. The EQE measurement system is Hamamatsu C9920-12, which equipped with Hamamatsu PMA-12 Photonic multichannel analyzer C10027-02 whose longest detection wavelength is 1100 nm.

1.7 Synthesis

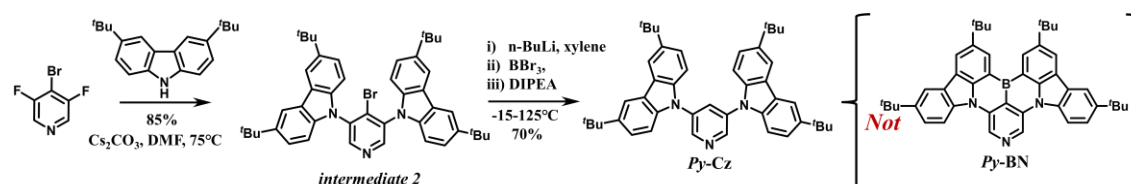


Scheme S1. Synthetic procedures of *Py-Cz-BN*.

9,9',9'',9'''-(4-bromopyridine-2,3,5,6-tetrayl)tetrakis(3,6-di-tert-butyl-9H-carbazole) (intermediate 1) : A mixture of 3,6-di-tert-butyl-9H-carbazole (2.44 g, 8.76 mmol), 4-bromo-2,3,5,6-tetrafluoropyridine (0.5 g, 2.19 mmol) and Cs_2CO_3 (5.69 g, 17.5 mmol) in dry DMF (40 mL) was stirred at 75°C for 6 h. After cooling to room temperature, the reaction mixture was added into a large amount of methanol, precipitate appeared immediately, yellow solid was obtained after filtration. Then, the yellow solid was washed with water and dried under high vacuum. Finally, the crude product was purified by column chromatography on silica gel (eluent: hexane/dichloromethane = 10:1, v/v) to afford intermediate 1 as a yellow solid (yield = 1.94 g, 70%). $^1\text{H NMR}$ (400 MHz, CD_2Cl_2): δ = 7.74 (d, J = 1.8 Hz, 4H), 7.66 (d, J = 1.9 Hz, 4H), 7.30 (s, 2H), 7.28 (s, 2H), 7.17 (d, J = 1.8 Hz, 2H), 7.15 (d, J = 1.9 Hz, 2H), 7.05 (s, 4H), 7.02 (s, 4H), 1.39 (s, 37H), 1.36 (s, 36H). MS (MALDI-TOF): m/z [M^+] calculated for $\text{C}_{85}\text{H}_{97}\text{BrN}_5$ 1266.4238; found, 1266.4236.

Synthesis of Py-Cz-BN: To a solution of intermediate 1 (621 mg, 0.48 mmol) in dry *o*-xylene (40 mL) was slowly added $n\text{-BuLi}$ (1.6 M in hexane, 0.45 mL, 0.72 mmol) at -15°C . After reacting for 2 h at room temperature, BBr_3 (0.114 mL, 1.2 mmol) was slowly added at -15°C , and then the mixture was stirred at 60°C for 3 h. After adding $\text{NEt}(\text{i-Pr})_2$ (0.3 mL, 1.8 mmol) at room temperature, the reaction mixture was further stirred at 125°C for 12 h. After cooling to room temperature, the reaction mixture was quenched by the addition of water, and then extracted with CH_2Cl_2 . The combined organic layer was dried over anhydrous MgSO_4 . After filtration and evaporation, the crude product was

purified by silica gel column chromatography (eluent: hexane/CH₂Cl₂ = 10:1, v/v) and recrystallization from CH₂Cl₂/methanol to afford *Py-Cz-BN* as a pink solid (yield = 458 mg, 80%). ¹H NMR (400 MHz, CDCl₃) δ 9.12 (d, *J* = 1.8 Hz, 2H), 8.47 (d, *J* = 1.8 Hz, 2H), 7.98 (s, 4H), 7.83 (d, *J* = 1.8 Hz, 2H), 7.26 (m, 4H), 7.11 (s, 4H), 6.74 (d, *J* = 8.8 Hz, 2H), 6.51 (dd, *J* = 8.8, 2.0 Hz, 2H), 1.73 (s, 18H), 1.38 (s, 36H), 1.20 (s, 18H). ¹³C NMR (101 MHz, CDCl₃) δ 145.66, 144.96, 143.72, 142.08, 137.51, 137.23, 129.49, 129.33, 125.52, 125.33, 124.85, 124.06, 123.83, 123.53, 122.26, 121.70, 115.80, 115.67, 112.94, 111.50, 35.48, 34.81, 34.56, 32.37, 32.05, 31.68, 29.86, 27.07. MS (MALDI-TOF): *m/z* [M⁺] calculated for C₈₅H₉₅BN₅ 1195.9009; found, 1195.9008. Analytically calculated (%) for C₈₅H₉₄BN₅: C, 85.32; H, 7.92; N, 5.85; found: C, 85.33; H, 7.91; N, 5.85.



Scheme S2. Synthetic procedures of *Py-Cz* (*Py-BN*).

9,9'-(4-bromopyridine-3,5-diyl)bis(3,6-di-tert-butyl-9H-carbazole)

(*intermediate 2*) : A mixture of 3,6-di-tert-butyl-9H-carbazole (2.90 g, 10.4 mmol), 4-bromo-3,5-difluoropyridine (1.0 g, 5.2 mmol) and Cs₂CO₃ (6.76 g, 20.8 mmol) in dry DMF (30 mL) was stirred at 75 °C for 6 h. After cooling to room temperature, the reaction mixture was added into a large amount of methanol, precipitate appeared immediately, white solid was obtained after filtration. Then, the white solid was washed with water and dried under high vacuum. Finally, the crude product was purified by column chromatography on silica gel (eluent: hexane/dichloromethane = 10:1, v/v) to afford intermediate 2 as a white solid (yield = 3.14 g, 85%). ¹H NMR (400 MHz, CD₂Cl₂): δ 8.83 (s, 2H), 8.20 (s, 4H), 7.55 (d, *J* = 8.4 Hz, 4H), 7.15 (d, *J* = 10.2 Hz, 4H), 1.47 (s, 36H). MS (MALDI-TOF): *m/z* [M⁺] calculated for C₄₅H₅₁BrN₃ 712.3263; found, 712.3262.

Synthesis of Py-Cz: To a solution of intermediate 2 (640 mg, 0.9 mmol) in dry o-xylene (20 mL) was slowly added *n*-BuLi (1.6 M in hexane, 0.84 mL, 1.35 mmol) at -15 °C. After reacting for 2 h at room temperature, BBr₃ (0.22 mL, 2.25 mmol) was slowly added at -15 °C, and then the mixture was stirred at 60 °C for 3 h. After adding NEt(*i*-Pr)₂ (0.56 mL, 3.38 mmol) at room temperature, the reaction mixture was further stirred at 125 °C for 12 h. After cooling to room temperature, the reaction mixture was quenched by the addition of water, and then extracted with CH₂Cl₂. The combined organic layer was dried over anhydrous MgSO₄. After filtration and evaporation, the crude product was purified by silica gel column chromatography (eluent: hexane/CH₂Cl₂ = 10:1, v/v) and recrystallization from CH₂Cl₂/methanol to afford Py-Cz as a white solid (yield = 398 mg, 70%). ¹H NMR (400 MHz, CDCl₃) δ 8.97 (d, J = 2.2 Hz, 2H), 8.21 (s, 1H), 8.16 (d, J = 1.4 Hz, 4H), 7.52 (dd, J = 8.7, 1.8 Hz, 4H), 7.46 (d, J = 8.6 Hz, 4H), 1.47 (s, 36H). ¹³C NMR (101 MHz, CDCl₃) δ 145.82, 144.16, 138.81, 136.10, 130.98, 124.26, 124.14, 116.75, 108.96, 34.96, 32.11. MS (MALDI-TOF): *m/z* [M⁺] calculated for C₄₅H₅₂N₃ 633.4264; found, 633.4263. Analytically calculated (%) for C₄₅H₅₁N₃: C, 85.26; H, 8.11; N, 6.63; found: C, 85.27; H, 8.10; N, 6.63.

2. Other supplementary figures and tables

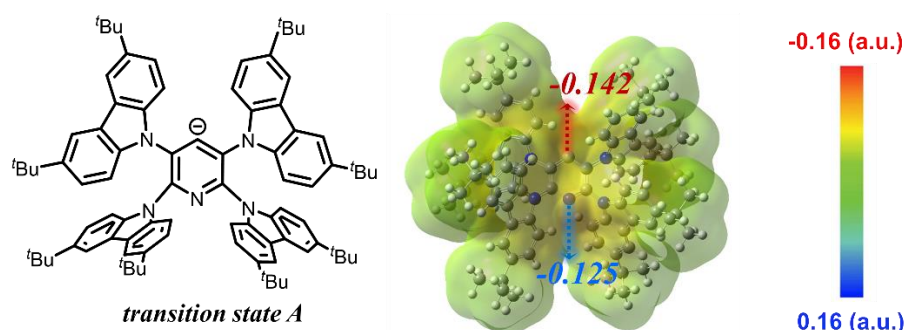


Fig. S1 Electrostatic potential map of transition state, calculated by the B3LYP/6-31G(d) method.

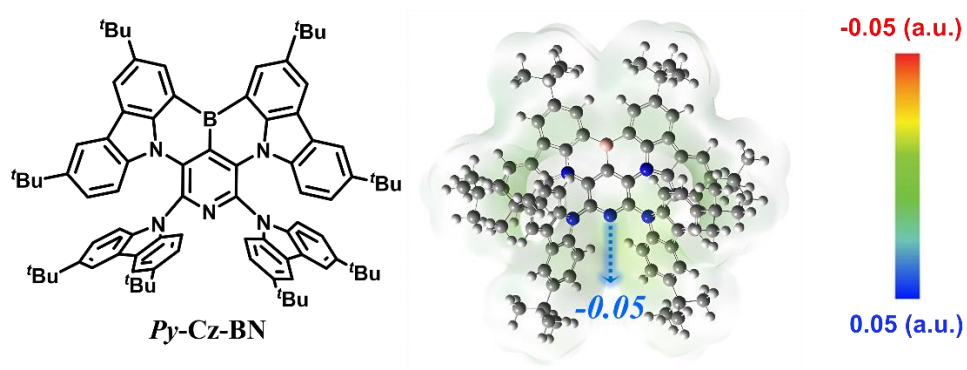


Fig. S2 Electrostatic potential map of *Py-Cz-BN*, calculated by the B3LYP/6-31G(d) method.

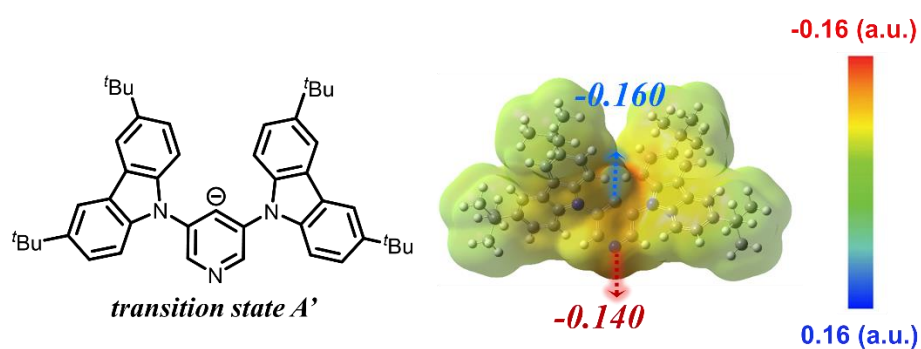


Fig. S3 Electrostatic potential map of *transition state A'*, calculated by the B3LYP/6-31G(d) method.

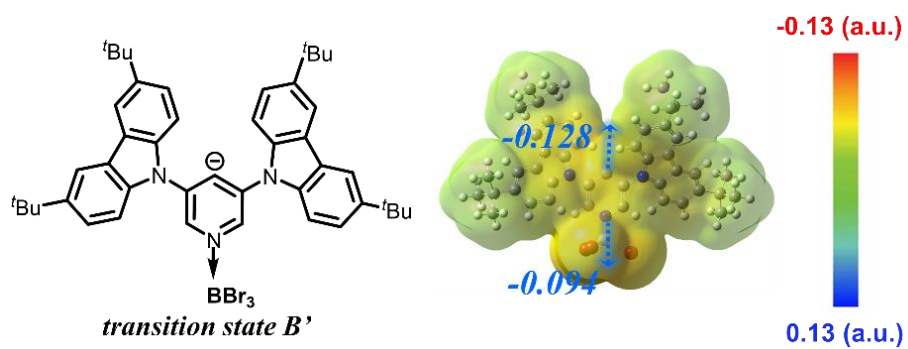


Fig. S4 Electrostatic potential map of transition state B', calculated by the B3LYP/6-31G(d) method.

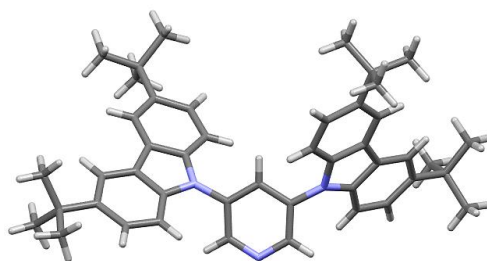


Fig. S5 The crystal structure of *Py-Cz*.

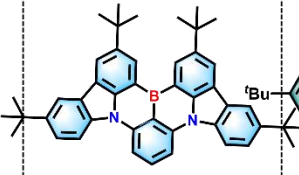
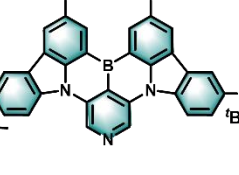
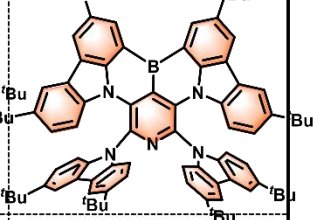
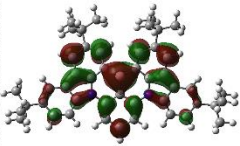
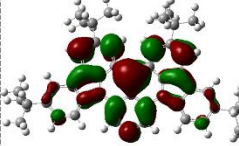
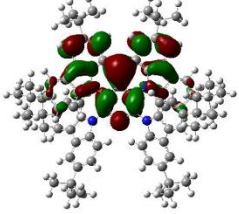
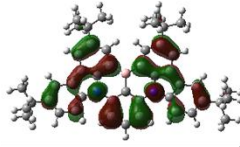
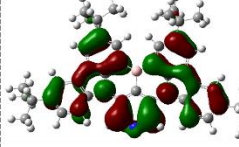
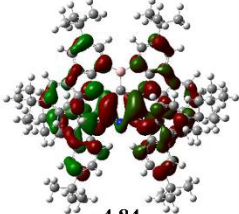
Compound	BCz-BN	Py-BN	Py-Cz-BN
Structure			
LUMO (eV)	 -1.63	 -1.95	 -1.83
HOMO (eV)	 5.05	 - 5.18	 -4.84
S_i/T_i (eV)	2.86 / 2.45	2.34 / 2.31	2.34 / 1.98
f	0.4125	0.4420	0.2644
FWHM (nm/eV)	16 / 0.09	17 / 0.09	28 / 0.12

Fig. S6 Molecular structures, HOMO/LUMO distributions and calculated excited states at the B3LYP/6-31G (d) level for the compounds.

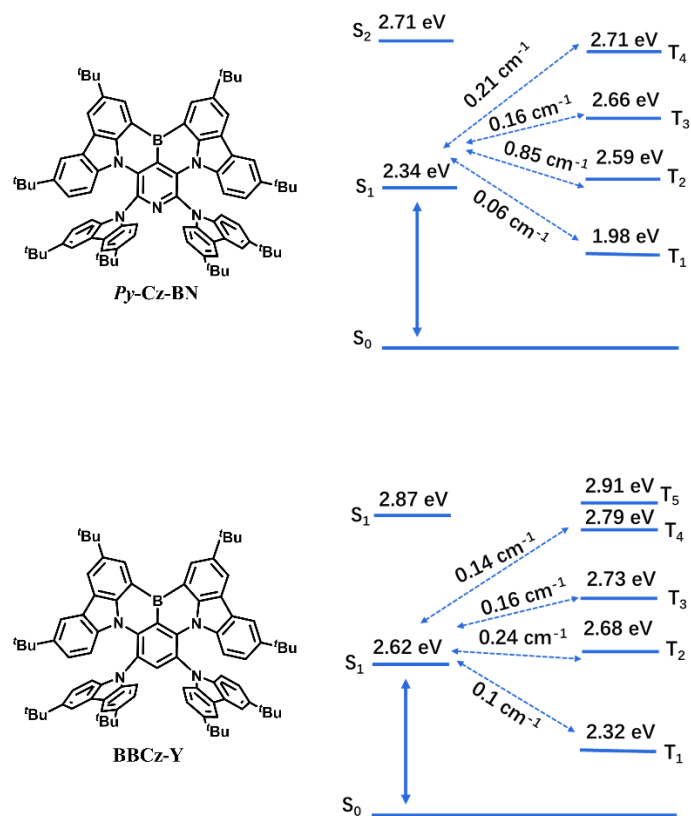


Fig. S7 Spin-orbit coupling (SOC) matrix elements between the T_n and S_n states of Py-Cz-BN and BBCz-Y.

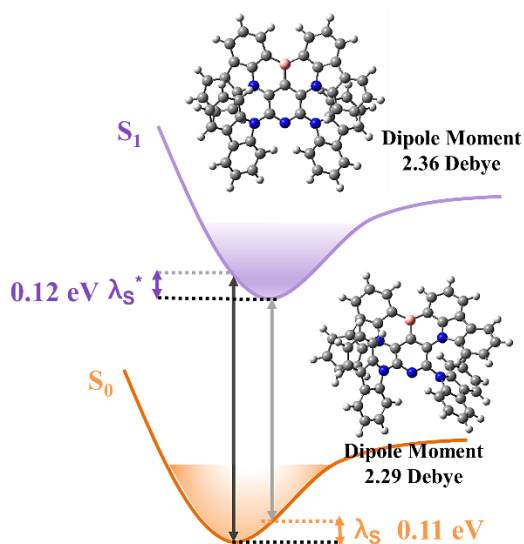


Fig. S8 The optimized S_0 and S_1 structures of Py-Cz-BN and reorganization energies, calculated by the PBE0/6-31G(d) method.

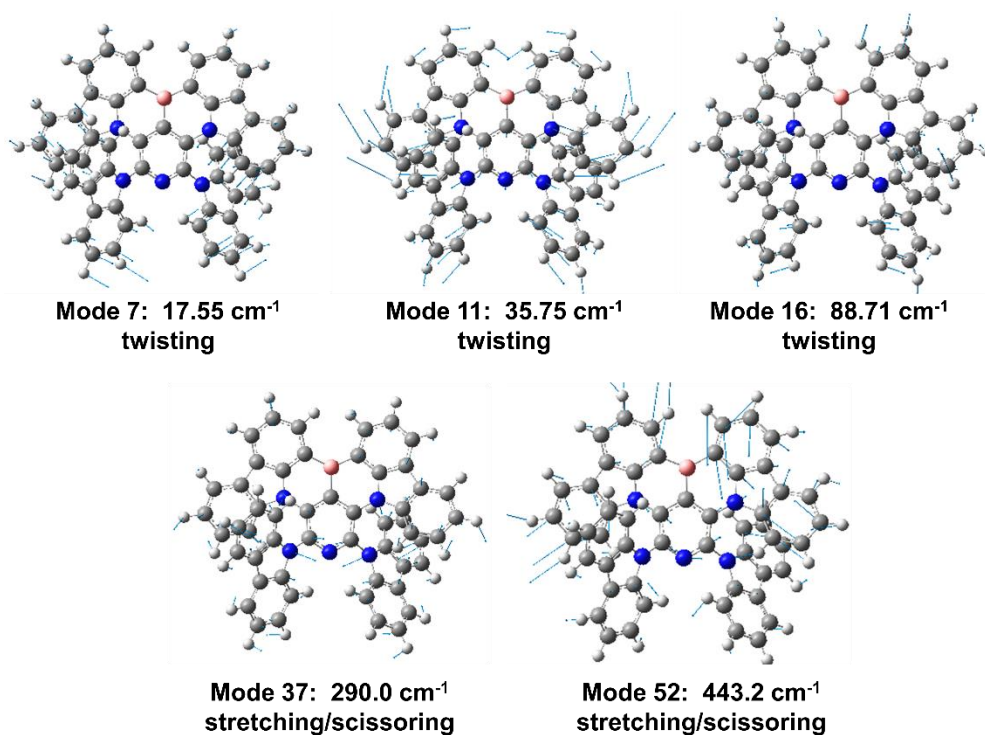


Fig. S9 Vibrational modes in the S_0 state involved in the Franck-Condon spectral progression of *Py-Cz-BN* at the (TD)B3LYP/6-31G(d) level.

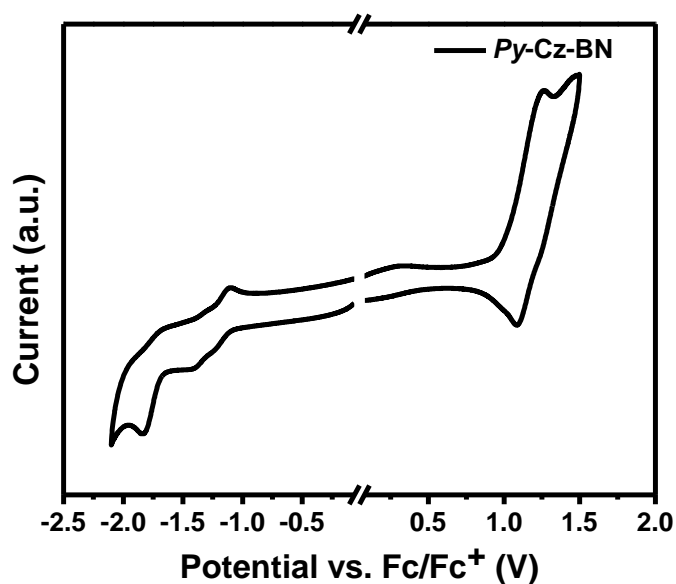


Fig. S10 Cyclic voltammogram of *Py-Cz-BN*.

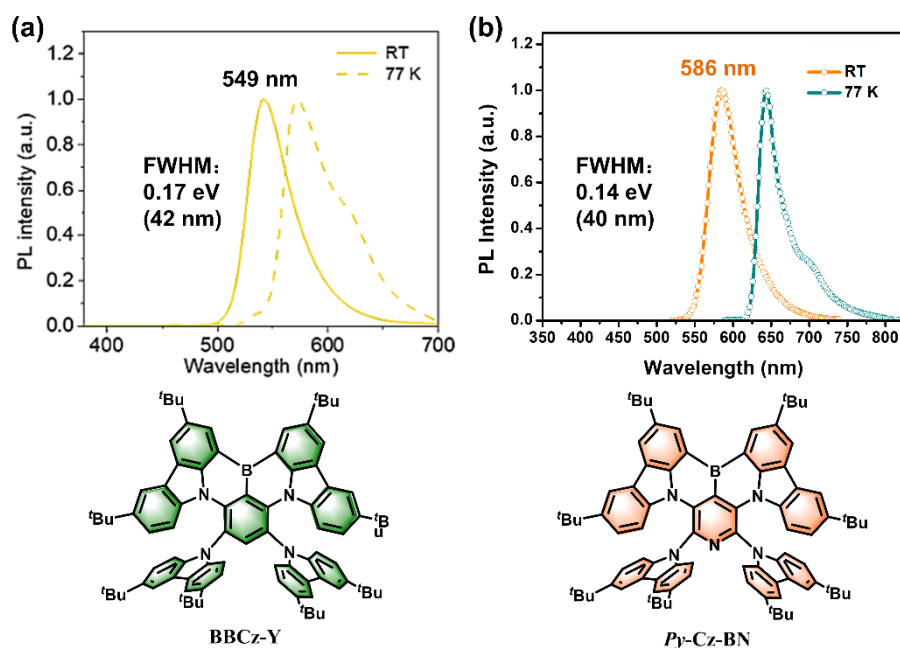


Fig. S11 Fluorescence (300 K) and phosphorescence (77 K) spectra of BBCz-Y (a) and Py-Cz-BN (b) in toluene solutions (10^{-5} M).

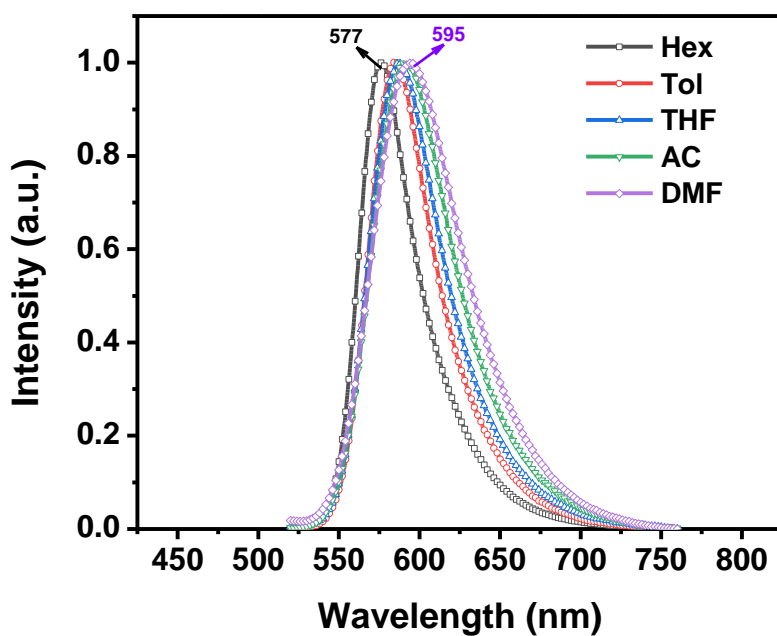


Fig. S12 Normalized PL spectra of Py-Cz-BN in different solvents.

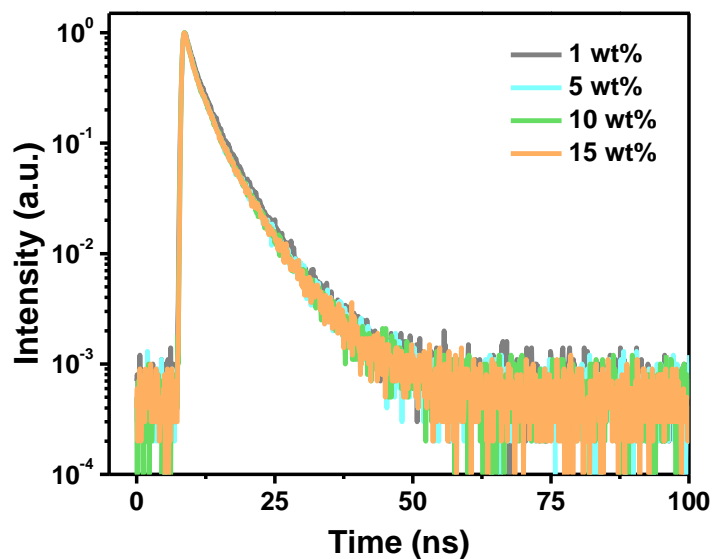


Fig. S13 Prompt PL decays of the doped films with different dopant concentrations in mCBP: x wt% *Py-Cz-BN* ($x=1, 5, 10, 15$) in the nanosecond range.

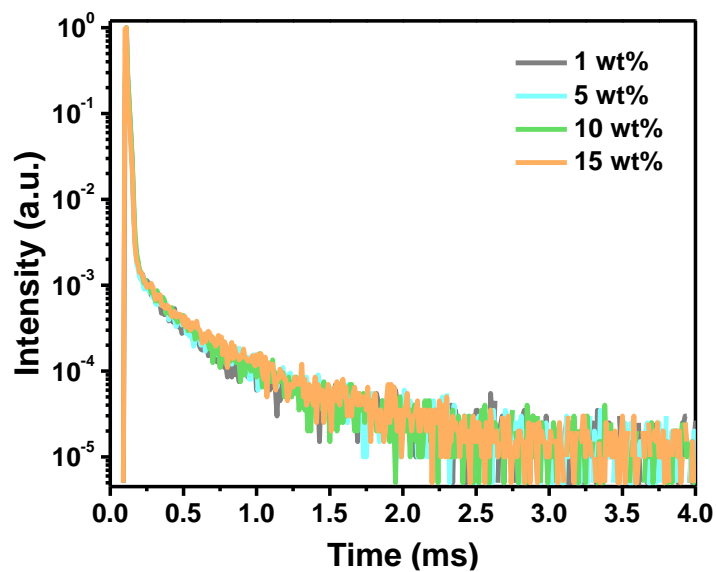


Fig. S14 Transient PL decay curves of the doped films with different dopant concentrations in mCBP: x wt% *Py-Cz-BN* ($x=1, 5, 10, 15$).

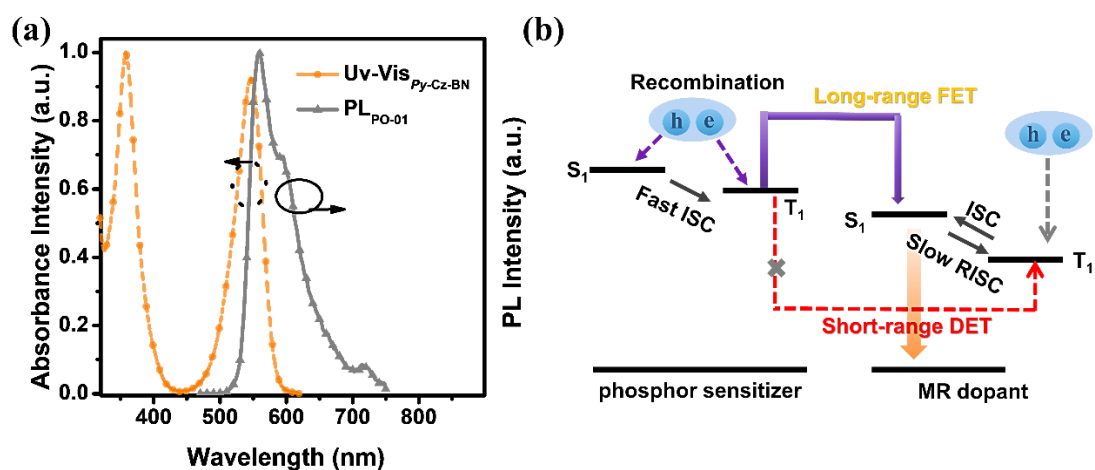


Fig. S15 (a) The emission spectrum of PO-01 and the absorption spectra of $Py-Cz-BN$ measured in dilute toluene solution. (b) The emission mechanism of phosphorescence sensitized MR emitter process (FET: förster energy transfer; RISC: reverse intersystem crossing).

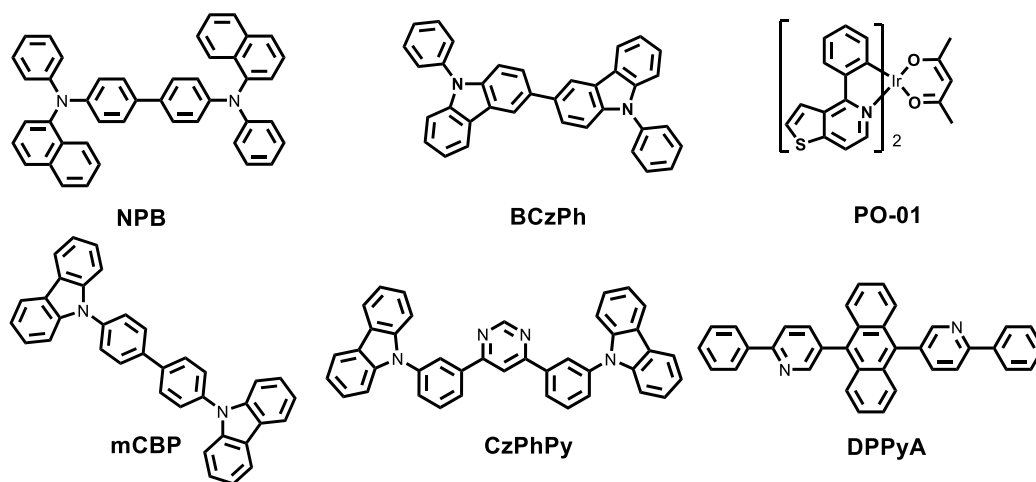


Fig. S16 Molecular structures of the materials used in phosphorescence sensitized $Py-Cz-BN$ devices.

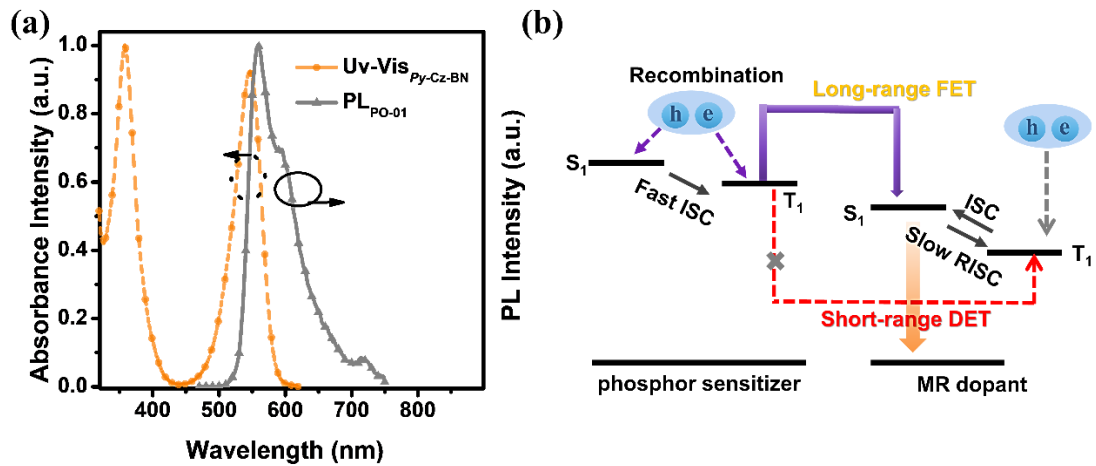


Fig. S16 (a) The emission spectrum of PO-01 and the absorption spectra of *Py-Cz-BN* measured in dilute toluene solution. (b) The emission mechanism of phosphorescence sensitized MR emitter process (FET: förster energy transfer; RISC: reverse intersystem crossing).

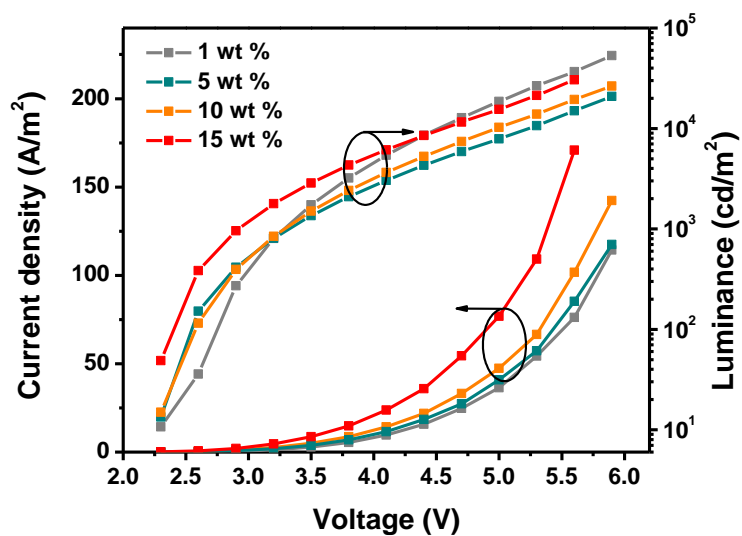
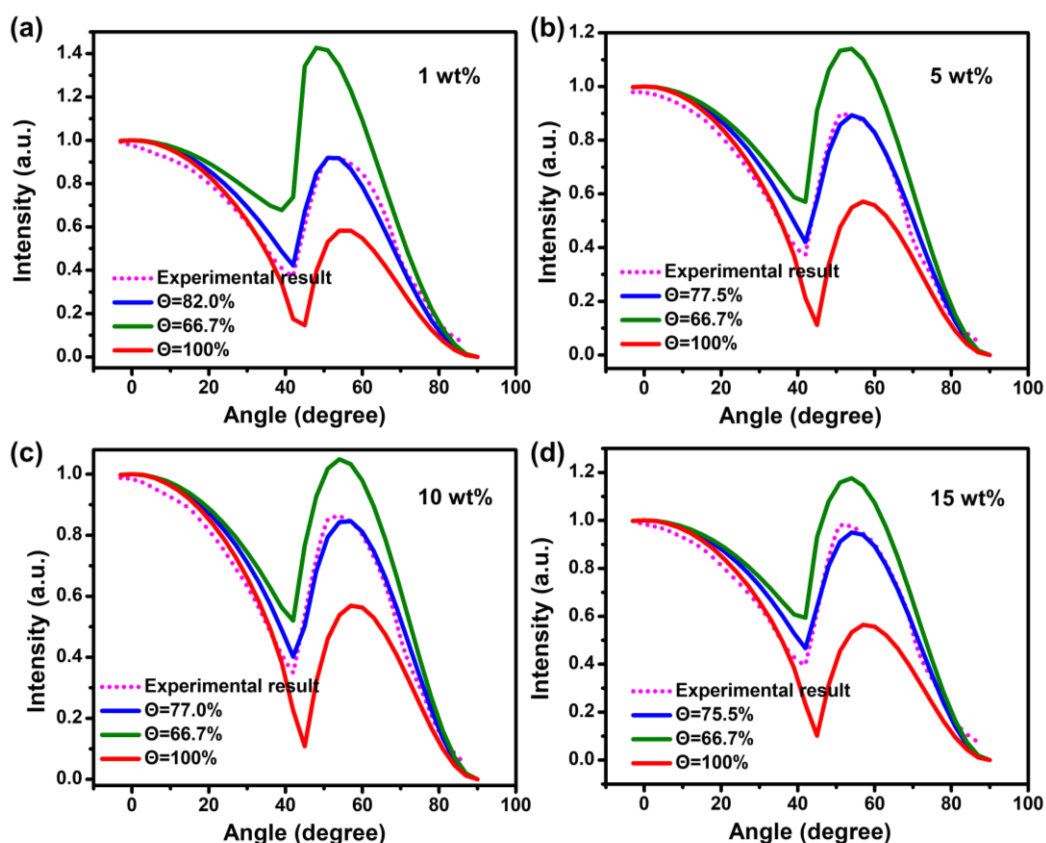


Fig. S17 Current density-voltage-luminance characteristics of phosphorescence sensitized *Py-Cz-BN* devices.

Table S1 Summary of the EL data of phosphorescence sensitized *Py-Cz-BN* devices.

Device	$\lambda_{EL}^{a)}$ [nm]	FWHM ^{b)} [eV]	FWHM ^{b)} [nm]	$V_{turn-on}^{c)}$ [V]	EQE ^{d)} [%]	CIE ^{e)} (x,y)
1 wt%	587	0.18	54	2.2	29.6/23.6/20.0	0.55,0.45
5 wt%	594	0.18	54	2.2	28.1/18.7/12.1	0.59,0.41
10 wt%	597	0.18	54	2.2	26.9/18.2/11.5	0.60,0.40
15 wt%	598	0.18	54	2.2	25.3/17.4/11.0	0.60,0.40

^{a)}Maximum electroluminescence wavelength. ^{b)}Full width at half maximum of electroluminescence. ^{c)}Turn-on voltage when brightness is 0.2 cd m⁻². ^{d)}Maximum efficiency/efficiency at 1000 cd m⁻²/ efficiency at 5000 cd m⁻². ^{e)}Recorded at 10 mA/cm².

**Fig. S18** Angle-dependent PL spectra of the doped films with different dopant concentrations in mCBP: x wt% *Py-Cz-BN* (x=1, 5, 10, 15).

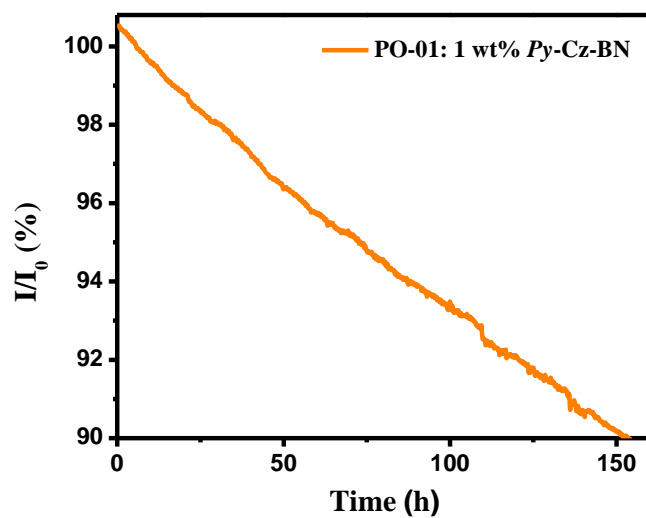


Fig. S19 The device (phosphorescence sensitized *Py-Cz-BN* device) luminance versus lifetime curve measured under 5 000 cd/m^2 .

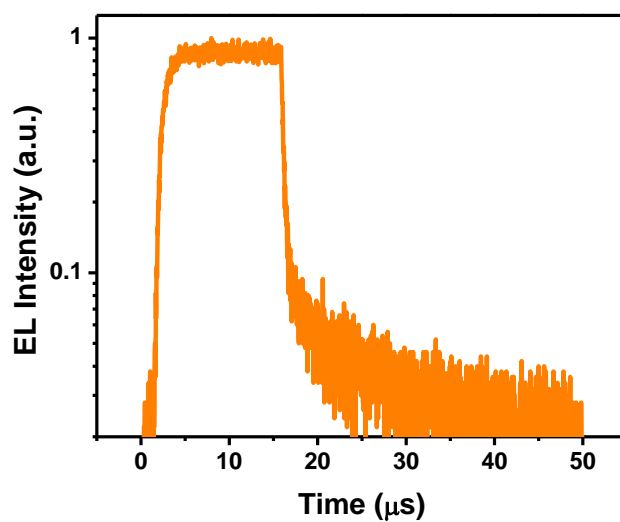


Fig. S20 The transient EL decay curve of the 1 wt% doped device (EML: mCBP: 20 wt% PO-01: 1 wt% *Py-Cz-BN*).

Table S2 Crystal Data and Structure Refinement of *Py-Cz-BN*.

	<i>Py-Cz-BN</i>
Formula	C ₈₅ H ₉₄ BN ₅
molecular weight	1196.46
crystal system	triclinic
space group	P-1
crystal size [mm ³]	0.15 × 0.13 × 0.12
a [Å]	13.9175(4)
b [Å]	14.8192(4)
c [Å]	19.2412(5)
α [°]	89.702(2)
β [°]	77.628(2)
γ [°]	79.792(2)
V [Å ³]	3812.69(18)
Z	2
ρ _{calc} [g cm ⁻³]	1.042
temp [K]	172.99(10)
μ [mm ⁻¹]	0.452
reflections collected	78964
independent reflections	15613 [R _{int} = 0.0347, R _{sigma} = 0.0295]
RF, R _w (F ²) (all data)	R ₁ = 0.0656, wR ₂ = 0.1843
RF, R _w (F ²) [I > 2σ(I)]	R ₁ = 0.0740, wR ₂ = 0.1923
GOF	1.037
CCDC	2297213

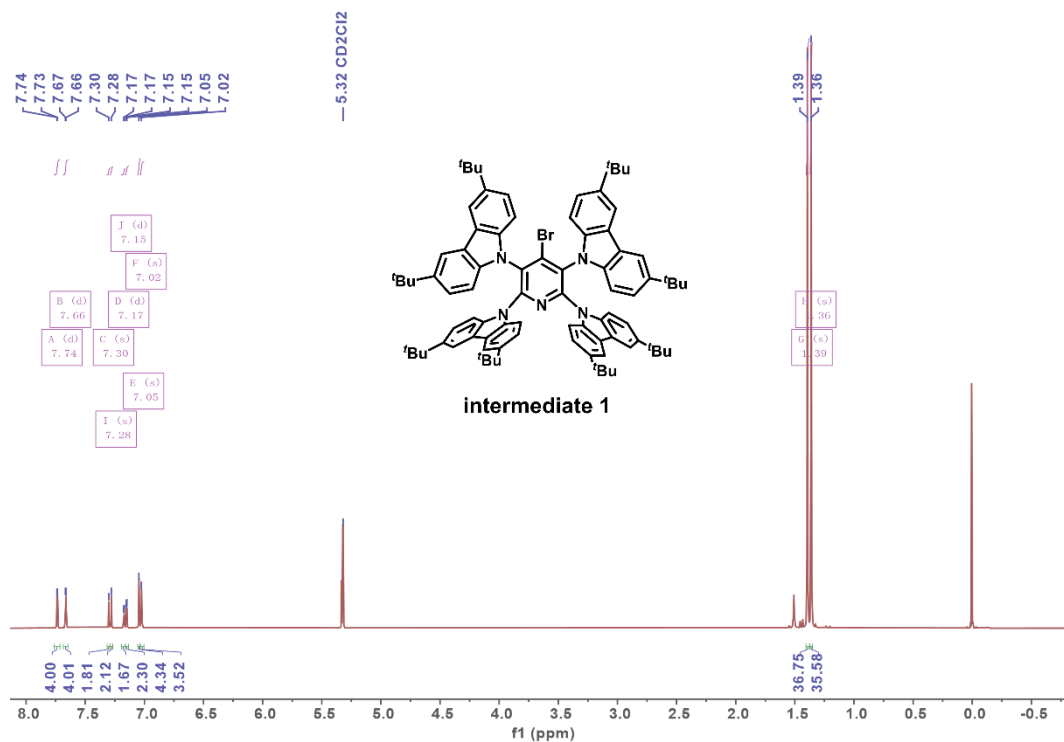


Fig. S21 ^1H NMR spectrum of intermediate 1 in CD_2Cl_2 .

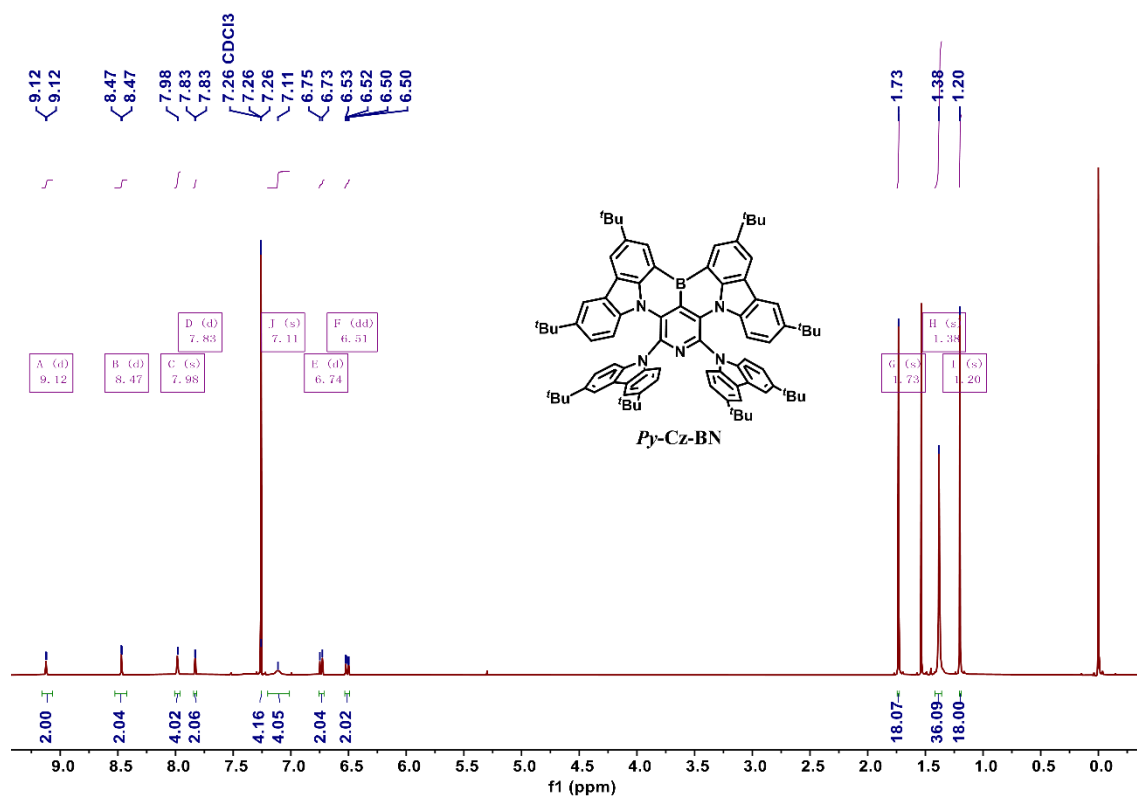


Fig. S22 ^1H NMR spectrum of Py-Cz-BN in CDCl_3 .

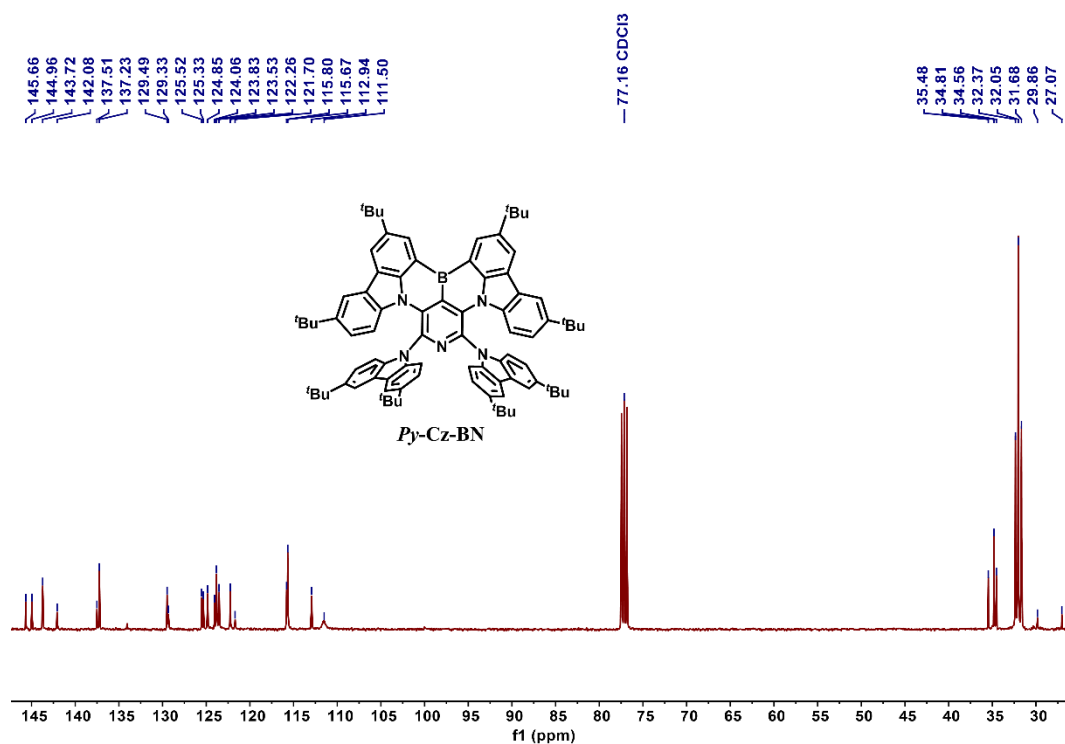


Fig. S23 ¹³C NMR spectrum of *Py-Cz-BN* in CDCl₃.

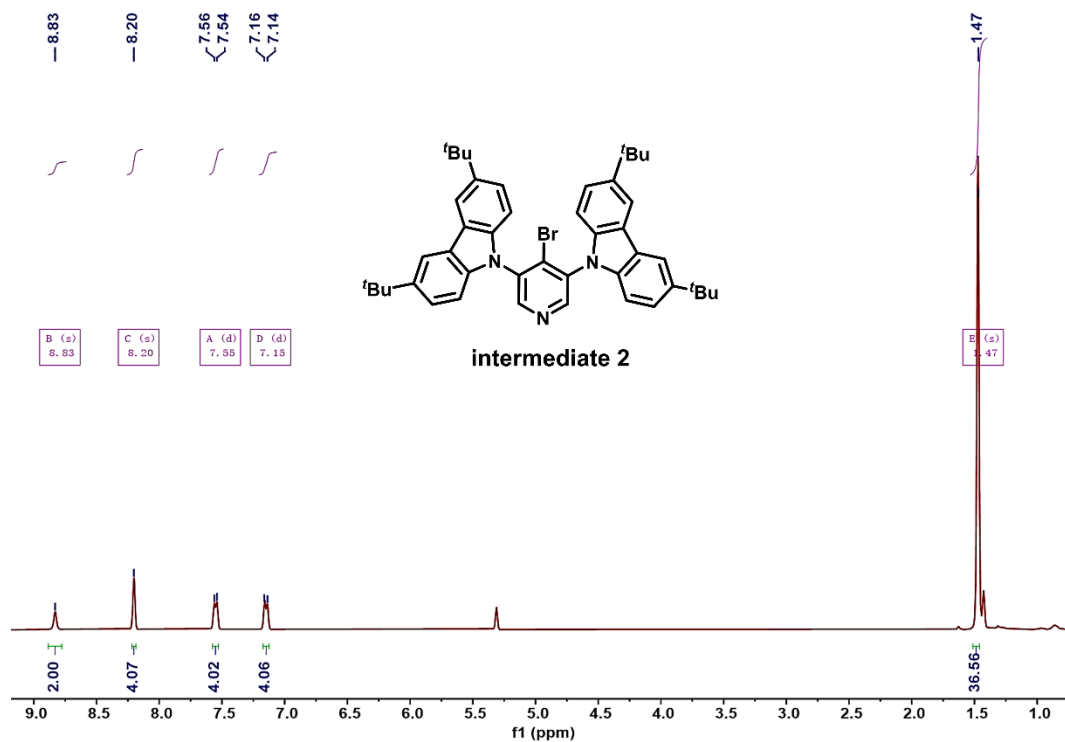


Fig. S24 ¹H NMR spectrum of *intermediate 2* in CD₂Cl₂.

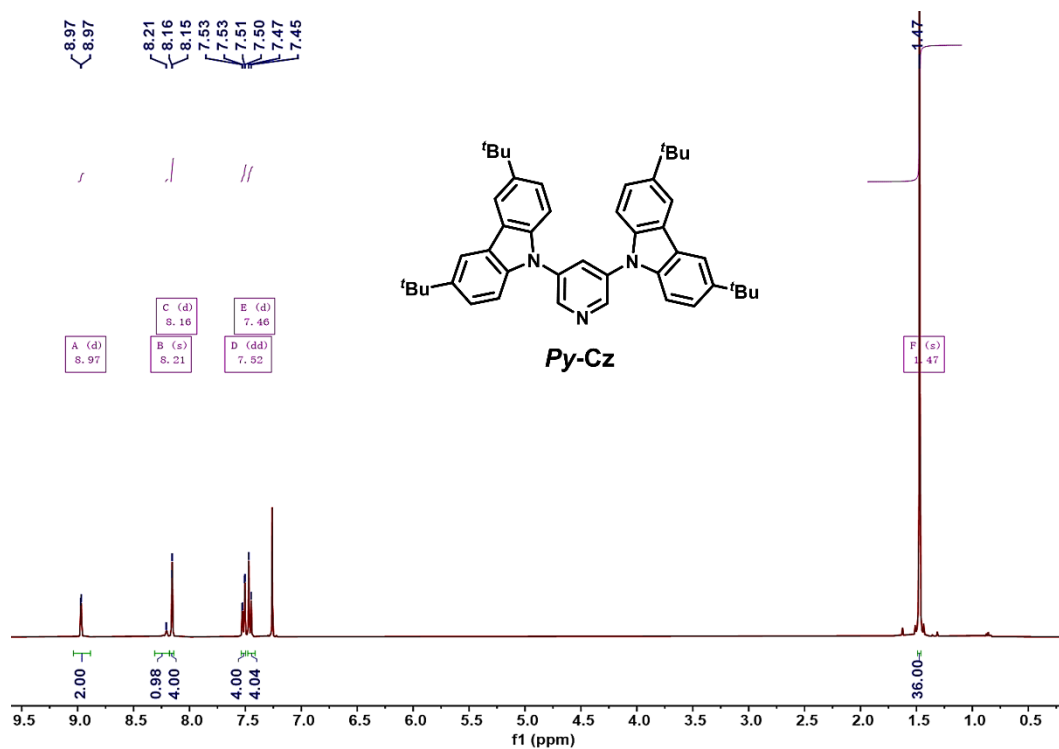


Fig. S25 ¹H NMR spectrum of *Py-Cz* in CDCl₃.

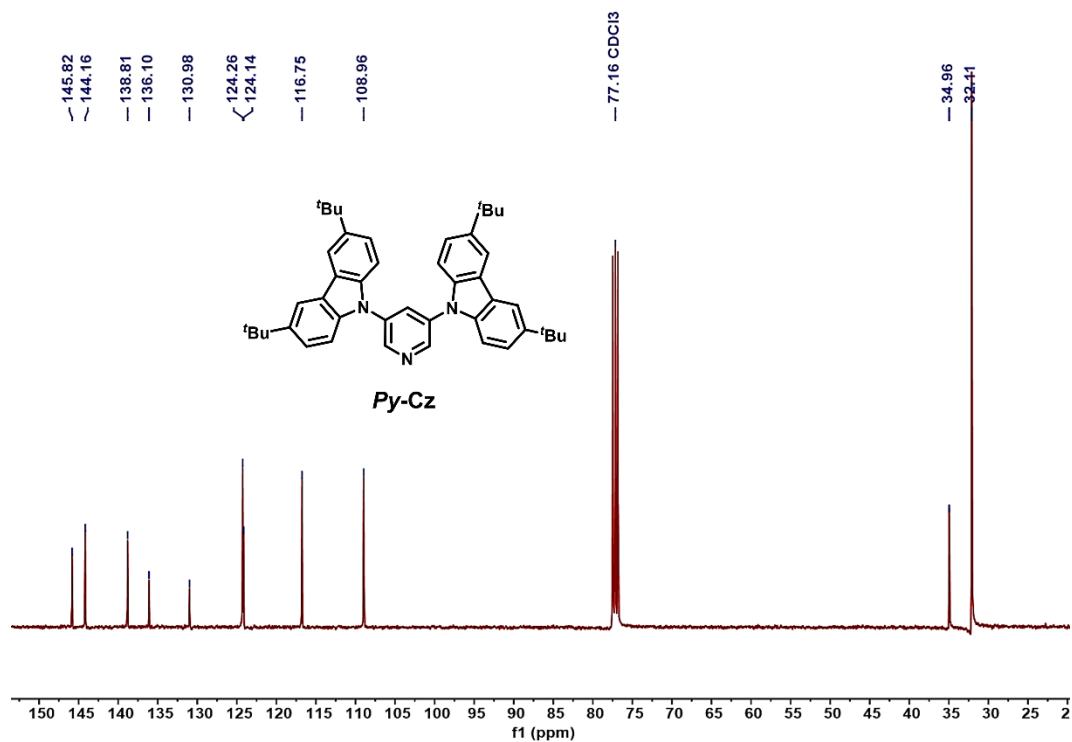


Fig. S26 ¹³C NMR spectrum of *Py-Cz* in CDCl₃.

3. Reference

- S1. Gaussian 09, Revision A.02, M. J. Frisch, G. W. Trucks, H. B. Schlegel, G. E. Scuseria, M. A. Robb, J. R. Cheeseman, G. Scalmani, V. Barone, G. A. Petersson, H. Nakatsuji, X. Li, M. Caricato, A. Marenich, J. Bloino, B. G. Janesko, R. Gomperts, B. Mennucci, H. P. Hratchian, J. V. Ortiz, A. F. Izmaylov, J. L. Sonnenberg, D. Williams-Young, F. Ding, F. Lipparini, F. Egidi, J. Goings, B. Peng, A. Petrone, et al., *Gaussian, Inc.*, Wallingford, CT 2016.
- S2. M. Ernzerhof, G.E. Scuseria, Assessment of the Perdew-Burke-Ernzerhof exchange-correlation functional, *J. Chem. Phys.*, 1999, **110**, 5029–5036.
- S3. C. Adamo, V. Barone, Toward reliable density functional methods without adjustable parameters: The PBE0 model, *J. Chem. Phys.*, 1999, **110**, 6158–6169.
- S4. J.P. Perdew, K. Burke, M. Ernzerhof, Generalized gradient approximation made simple, *Phys. Rev. Lett.*, 1996, **77**, 3865–3868.
- S5. J.P. Perdew, K. Burke, M. Ernzerhof, Errata: Generalized gradient approximation made simple, *Phys. Rev. Lett.*, 1997, **78**, 1396.
- S6. Y. Kondo, K. Yoshiura, S. Kitera, H. Nishi, S. Oda, H. Gotoh, Y. Sasada, M. Yanai, T. Hatakeyama, *Nat. Photonics*, 2019, **13**, 678-682.